PHYSICAL REVIEW B **82**, 140103(R) (2010)

Probing ferroelectricity in $PbZr_{0.2}Ti_{0.8}O_3$ with polarized soft x rays

E. Arenholz,[1] G. van der Laan,[2] A. Fraile-Rodríguez,[3] P. Yu,[4] Q. He,[4] and R. Ramesh[4]
[1]*Advanced Light Source, Lawrence Berkeley National Laboratory, Berkeley, California 94720, USA*
[2]*Diamond Light Source, Chilton, Didcot, Oxfordshire OX11 0DE, United Kingdom*
[3]*Swiss Light Source, Paul Scherrer Institut, CH 5232 Villigen, Switzerland*
[4]*Department of Materials Science and Engineering and Department of Physics, University of California, Berkeley, California 94720, USA*
(Received 11 October 2010; published 26 October 2010)

The reduction in symmetry associated with the onset of ferroelectric order in $PbZr_{0.2}Ti_{0.8}O_3$ (PZT) thin films leads to a pronounced difference at the Ti $L_{3,2}$ absorption edges between spectra measured with the x-ray linear polarization perpendicular and parallel to the ferroelectric polarization. We introduce a general method to analyze the observed difference spectra using atomic multiplet calculations. Moreover, we find experimental evidence for structural changes in PZT induced by the reversal of the ferroelectric polarization.

DOI: 10.1103/PhysRevB.82.140103 PACS number(s): 77.80.−e, 78.70.Dm, 77.84.Cg, 78.20.Bh

Ferroelectric oxides exhibit a spontaneous, stable, and switchable electric polarization that is due to atomic displacements of positive metallic ions and negative oxygen ions in opposite directions, which reduces the symmetry of the crystal lattice.[1] In thin films—especially important for applications such as nonvolatile memories[2]—interface and surface effects can dominate over the bulklike behavior of the film interior.[3] For example, strain induced by the lattice mismatch between substrate and film lead to enhanced ferroelectric polarization and transition temperature in $BaTiO_3$ on (110) $GdScO_3$ and (110) $DyScO_3$ substrates.[4] Experiments and calculations have shown that ferroelectric surfaces with opposite polarity have different characteristics for adsorbing molecules and catalytic activity.[5–7] Conversely, the chemical environment can control the polarization of a ferroelectric film by determining the ionic compensation at its surface.[8]

To shed light on the impact of ferroelectric order on the electronic and atomic structure in the surface near region of ferroelectric $PbZr_{0.2}Ti_{0.8}O_3$ (PZT) films deposited on $SrRuO_3$ (SRO) and $La_{0.7}Sr_{0.3}MnO_3$ (LSMO) electrodes, we employed soft x-ray absorption (XA) spectroscopy. We show that the reduction in symmetry around the Ti^{4+} ions has a pronounced impact on the Ti $L_{3,2}$ absorption edges which can be explained using atomic multiplet calculations. Moreover, we find experimental evidence for changes in the PZT structure induced by the reversal of the ferroelectric polarization.

(100)-oriented $SrTiO_3$ substrates were etched by buffered hydrofluoric acid (HF) and annealed in flowing oxygen at 1000 °C for 3 h. Bottom electrodes, 30 nm pseudomorphic layers of SRO and LSMO, were grown by pulsed laser deposition at 700 °C with oxygen pressure of 100 mTorr and 200 mTorr, respectively. 70–200-nm-thick PZT films were deposited on the electrodes at 630 °C in 100 mTorr of oxygen. Piezoforce microscopy (PFM) confirmed that the ferroelectric polarization in the PZT/SRO points away from the bottom electrode while it points toward the bottom electrode in PZT/LSMO.[9] XA experiments were performed on beamline 4.0.2 at the Advanced Light Source by recording the sample drain current as a function of photon energy.[10] Photoemission electron microscopy (PEEM) experiments were carried out on the SIM beamline at the Swiss Light Source.[11] All spectra were acquired at ambient temperature at pressures $\leq 5 \times 10^{-9}$ Torr with 100% linearly polarized x rays impinging at an angle of 16° to the sample surface probing the topmost 5–8 nm.

Figure 1(a) shows XA spectra obtained from PZT/SRO. The Ti $L_{3,2}$ spectrum exhibits the characteristic structure of a Ti^{4+} d^0 configuration[12] due to electric dipole transitions to $2p^5 3d^1$ final states. The $2p$ spin-orbit interaction splits the spectrum into $2p_{3/2}(L_3)$ and $2p_{1/2}$ (L_2) structures with energy separation of ~5.5 eV, which are further split by crystal-field interaction, i.e., the electrostatic potential, V, due to the neighboring lattice sites acting on the $3d$ orbitals. In octahedral (O) site symmetry the e orbitals of Ti point toward the oxygen ligands, while the t_2 orbitals point in between them, resulting in a lower energy for the latter. With increasing photon energy the four main peaks can therefore be labeled according to their main character as $2p_{3/2}3d(t_2)$, $2p_{3/2}3d(e)$, $2p_{1/2}3d(t_2)$, and $2p_{1/2}3d(e)$, cf., Fig. 1. None of these states is pure due to mixing by $2p$-$3d$ electrostatic interactions. Distortion of the Ti site from octahedral symmetry results in a nonsymmetric broadening of especially the $3d(e)$ peaks.[13] Lowering to tetragonal symmetry splits the $t_2(O)$ states into $b_2=d(xy)$ and $e=d(xz,yz)$ and the $e(O)$ states into $b_1=d(x^2-y^2)$ and $a_1=d(z^2)$. This gives a difference between XA spectra taken with polarization along the z and x,y directions, i.e., parallel and perpendicular to the surface normal. We observe a ±20% difference in the photon energy range of the $2p_{3/2}3d(t_2)$ peak [cf., Fig. 1(a)]. Smaller but still easily detectable intensity differences are found at higher photon energies.

Figure 1(b) displays local XA spectra and their difference obtained by PEEM in a 30 μm × 30 μm area of the PZT/SRO sample where the ferroelectric polarization was reversed using PFM to point toward the bottom electrode. The XA spectra show the same main features as the as grown sample but we note that the low-energy side of the $2p_{3/2}3d(e)$ features is enhanced. The difference spectrum is identical in shape and magnitude to the data obtained from the as grown sample.

In Fig. 1(c) the XA spectra and their difference obtained from PZT/LSMO are plotted. The ferroelectric polarization

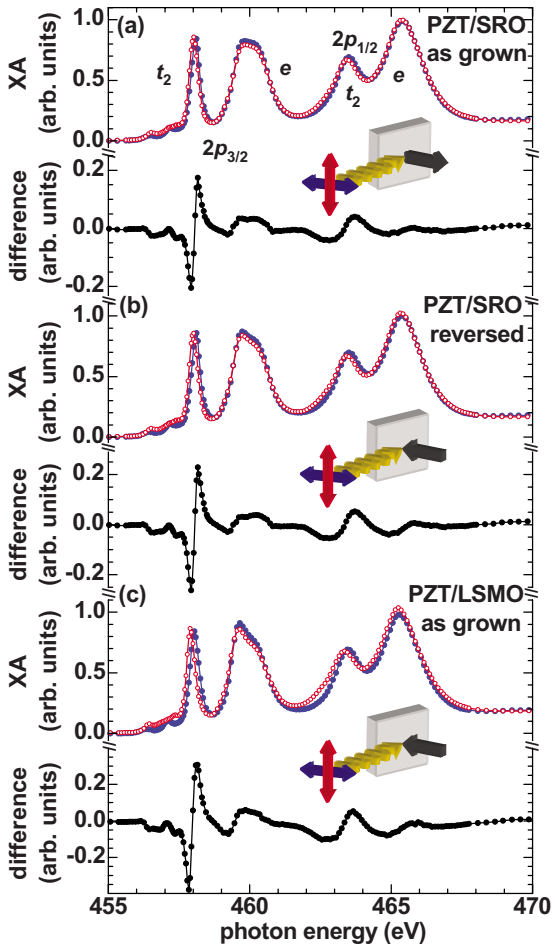

FIG. 1. (Color online) Experimental Ti $L_{3,2}$ XA and difference spectra of (a) PZT as grown on SRO, (b) PZT on SRO with reversed ferroelectric polarization, and (c) PZT as grown on LSMO. The ferroelectric polarization is indicated by a dark gray arrow in the insets, the incident x-ray beam by a gray (yellow) arrow and the x-ray polarization by (red) up-down and (blue) left-right arrows. Open (red) symbols indicate data obtained with the x-ray polarization aligned in the surface plane while the spectrum resulting with the x-ray polarization pointing out of the surface plane is shown by solid (blue) symbols.

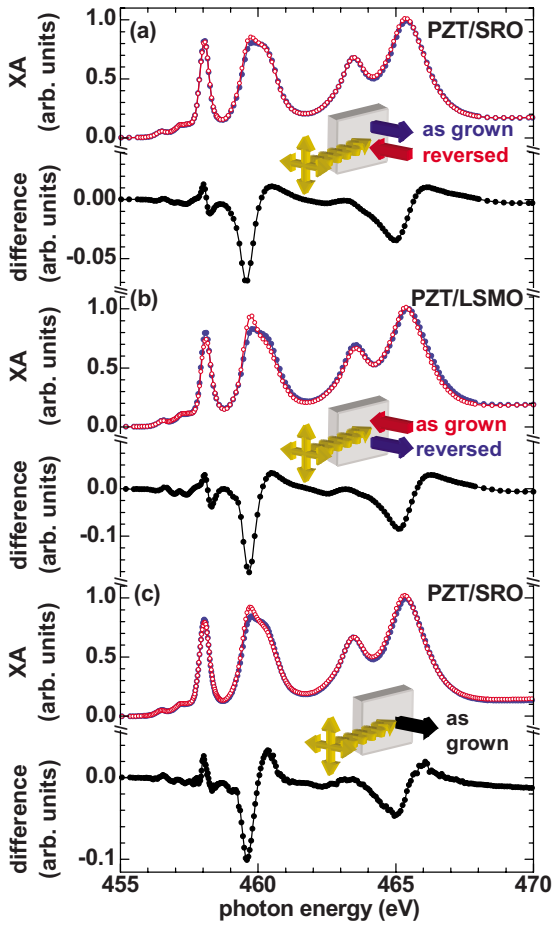

FIG. 2. (Color online) Polarization-averaged Ti $L_{3,2}$ XA and difference spectra of PZT. Solid (blue) symbols indicate data obtained with the ferroelectric polarization pointing away from the bottom electrode while the spectra resulting with the polarization pointing toward the electrode is shown by open (red) symbols for (a) SRO and (b) LSMO bottom electrodes. (c) Spectra for PZT/SRO with $c=0.414$ nm (solid [blue] symbols) and $c=0.416$ nm (open [red] symbols). The ferroelectric polarization is pointing away from the bottom electrode. Difference spectra are shown as black solid symbols. Insets depict experimental geometries described in Fig. 1.

in the as grown state of this system points toward the bottom electrode. The main features of the Ti $L_{3,2}$ XA spectra as well as the difference spectrum are the same as for the PZT/SRO system. An enhancement of the $2p_{3/2}3d(e)$ low-energy features is observed as in the case of PZT/SRO with the ferroelectric polarization pointing toward the bottom electrode.

To emphasize the difference in XA induced by the reversal of the ferroelectric polarization, Figs. 2(a) and 2(b) show a comparison of the XA results of PZT/SRO and PZT/LSMO, respectively, obtained from sample areas with opposite ferroelectric polarization. The data are the average of XA spectra obtained with the x-ray polarization aligned in the surface plane and perpendicular to it. We can rule out that a change in surface composition by the PFM tip is responsible for the difference spectra since XA spectra obtained from as grown and twice reversed areas of the sample resulting in same orientation of the ferroelectric polarization are identical. Moreover, PEEM images taken at the C K and O K edges do not show any significant differences between the as grown and reversed areas of the sample. The difference spectra in Figs. 2(a) and 2(b) have the same spectral shape, which shows unambiguously that they are caused the reversal of the ferroelectric polarization.

To understand the origin of the changes in XA spectral shape we performed atomic multiplet calculations, a powerful tool to obtain symmetry- and site-specific information of compounds with localized $3d^n$ electronic configurations. Calculations for the Ti XA spectrum, obtained using Cowan's code,[12,14,15] are shown in comparison with the experiments in Fig. 3. Although for Ti^{4+} compounds a good theoretical description of experiments is obtained for near cubic $SrTiO_3$ and rutile (D_{2h} symmetry),[13] calculating the detailed line shape of the $2p_{3/2}3d(e)$ peak remains in general an arduous task. Compared to other $3d^n$ configurations, a complication for $3d^0$ arises from the large distortion of the metal site due

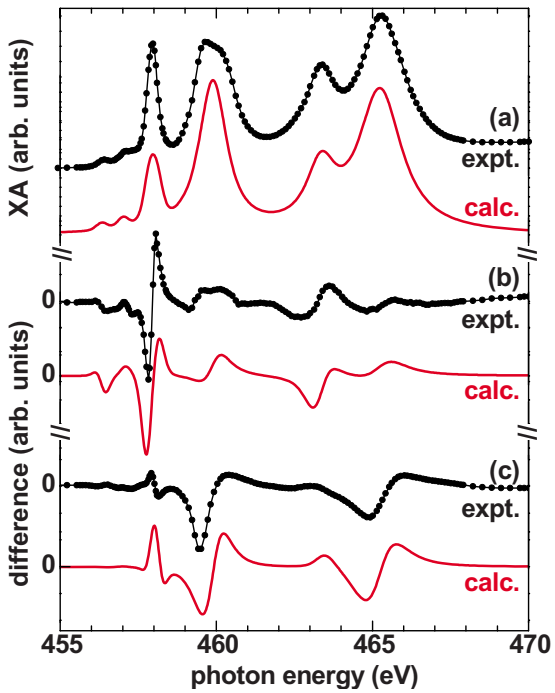

FIG. 3. (Color online) Comparison of experimental (symbols) and theoretical ([red] lines) results obtained at the Ti $L_{3,2}$ edges of PZT for (a) the XA spectrum, (b) the difference spectrum of XA spectra measured with the x-ray polarization perpendicular and parallel to the ferroelectric polarization, (c) the difference spectrum of XA spectra measured with the x-ray polarization collinear to the ferroelectric polarization pointing toward the sample surface and the bottom electrode. (b) and (c) show the calculated t_2- and e-split difference spectrum, respectively (defined as $I_z - I_x$ for $V_z > V_x$ in tetragonal symmetry).

to the absence of d-orbital bonding in the ground state; the same effect that is at the very origin of the ferroelectricity in Ti compounds. We therefore also performed cluster calculations[16] allowing a fractional d-electron count on the Ti site but this showed no significantly improved agreement. We therefore do not aim here to precisely reproduce all details within each peak. Instead, we present a general approach, relating the signature and sign of the difference spectrum to the character of the d state, which will allow us to obtain useful information about the local electronic structure.

It is at first sight rather surprising that the PZT measurements reveal two distinct difference spectra, i.e., a first difference spectrum between XA spectra obtained with the x-ray polarization parallel and perpendicular to the ferroelectric polarization (Fig. 1) and a distinct second difference spectrum between XA spectra with the ferroelectric polarization pointing toward the bottom electrode and away from it (Fig. 2). Since in tetragonal symmetry there can be only one linear dichroism spectrum, structural differences must be involved.

Taking the z axis along the tetragonal axis, we define the difference spectrum as $I_z - I_x$, where I_z (I_x) is the XA intensity obtained with the polarization vector along the $z(x)$ direction. In this difference spectrum the states with predominantly (xz,yz) and z^2 character of the created d electron show up as positive signals while those with predominantly xy and $x^2 - y^2$ character show up as negative signals. The t_2-e energy separation observed in the XA spectrum enables us to estimate the value of the cubic crystal-field parameter as $10Dq \approx 1.5$ eV. Tetragonal distortion leads to two additional crystal-field parameters, Ds and Dt, which allows us to decompose $I_z - I_x$ into two independent difference spectra. For small distortions the $I_z - I_x$ spectrum, which vanishes in cubic symmetry, is linear in both Ds and Dt. Any linear combination of Ds and Dt can be used to parametrize the difference spectrum, however, we will take—as what seems an arbitrary choice—those combinations that give an energy splitting in either the cubic t_2 or e state, i.e., $\Delta E(t_2) \equiv E(e) - E(b_2) = 5Dt - 3Ds$ and $\Delta E(e) \equiv E(a_1) - E(b_1) = -5Dt - 4Ds$. Thus, the t_2-split difference spectrum is obtained by introducing an energy splitting between the $e = d(xz,yz)$ and $b_2 = d(xy)$ levels while $\Delta E(e) = 0$. This represents the case that the plane normal to the z axis is distinct from the planes parallel to the z axis. The e-split difference spectrum is obtained by introducing an energy splitting between the $a_1 = d(z^2)$ and $b_1 = d(x^2 - y^2)$ levels while $\Delta E(t_2) = 0$. This means the z axis is distinct from the x and y axes, i.e., the electrostatic energy is different along z and x axes ($V_z \neq V_x$), corresponding to contraction or elongation of the z axis. Figures 3(b) and 3(c) show these two difference spectra, $I_z - I_x$, calculated in tetragonal symmetry for $V_z > V_x$, which means $d(xy)$ is the lowest level. For $V_z < V_x$, where $d(xz,yz)$ is the lowest level, the difference spectra keep the same shape but have opposite sign. It is seen that all four main peaks in both difference spectra have a $-/+$ signature for $V_z > V_x$ (and $+/-$ for $V_z < V_x$), which due to the relative energy differences between the levels. The spectra also nicely show the extent to which the t_2 and $e(O)$ states are intermixed: opening an energy gap in one of these states gives apart from a dispersive structure in the associated peaks also smaller features in the other peaks.

Returning to the experimental results in Fig. 1, PZT shows a strong polarization dependence in the $2p_{3/2}3d(t_2)$ peak, related to a splitting between $d(xy)$ and $d(xz,yz)$ levels. In the XA spectra the in-plane polarized peak has the lowest energy so that $d(xy)$ has the lowest energy. The spectral shape of the measured dichroism is in remarkably good agreement with the calculated t_2-split difference spectrum [Fig. 3(b)]. This is not a trivial result because, as mentioned above, the parameter choice in the calculation is an apparent arbitrary one. It demonstrates however that the linear dichroism originates primarily from a t_2 splitting, despite that the main bonding in the excited state is by $e(O)$ orbitals. This may be related to the fact that the Ti bond directions point out of the xy plane.

A strong point of the analysis using the difference spectra is the transferability of the method, as it does not depend on structural variations, such as between PZT/LSMO and PZT/SRO and it is also oblivious to variations in domain structures, as long as these are oriented mainly along one direction as in the present system. Such effects influence the XA spectra but not the generic shape of the difference spectrum.

Regarding the second difference spectrum (Fig. 2), the experimental XA shows a clear difference in PZT/SRO and PZT/LSMO between the x-ray polarization averaged spectra obtained with the ferroelectric polarization pointing toward the bottom electrode and away from it, notably in the

$2p_{3/2}3d(e)$ peak. To explain these differences in XA we have to assume that not only the electric polarization is reversed but that also the structure of the PZT has slightly changed. The observed difference spectrum agrees very well with the calculated e-split difference spectrum, $I_z - I_x$ for $V_z > V_x$. It can be seen from Fig. 2 that the $d(x^2-y^2)$ has lower energy than the $d(z^2)$ level for the polarization pointing toward the bottom electrode than away from it for both systems, PZT/SRO and PZT/LSMO. This is equivalent to an increase in the electrostatic potential along the z axis, such as caused by contraction along the z direction, in areas with the polarization pointing away from the bottom electrode compared to areas with the polarization pointing toward the bottom electrode. The fact that we use the difference spectrum again means that the results are rather insensitive to any structural or domain variations. We directly observe the difference between the average ensembles, while variations would not vanish in the individual spectra.

To confirm the presence of the structural changes, we compare the polarization averaged XA spectra of PZT/SRO systems with varying PZT layer thickness resulting in lattice constants $c=0.414$ and 0.416 nm as determined by x-ray diffraction. The samples are in the as grown state—i.e., the ferroelectric polarization points away from the bottom electrode. The results are shown in Fig. 2(c). We observe that the sample with $c=0.416$ nm—i.e., the sample with elongated c axis—shows the anticipated changes in the intensity of the $2p_{3/2}3d(e)$ feature. This clearly confirms our finding of the structural changes associated with the reversal of the ferroelectric polarization in PZT.

In conclusion, the ferroelectric order in PZT thin films leads to pronounced differences in the Ti^{4+} $L_{3,2}$ absorption between spectra measured with the x-ray polarization perpendicular and parallel to the ferroelectric polarization. We have introduced a general method to analyze the difference spectra, independent of the tetragonal crystal-field parameter values, by relating the $3d$-orbital character in the final state to the signature and sign of the difference spectra. This pronounced linear polarization dependence is a general phenomenon that we expect to find in any ferroelectric and multiferroic system. It will allow the study of ferroelecticity using soft x-ray spectroscopy and microscopy techniques with nanometer spatial resolution and on ultrafast times scales in an element-, valence-, and even site-resolved way. The availability of these tools will be crucial for the development of ferroelectric and multiferroic materials for applications.

Supported by the U.S. Department of Energy under Contract No. DE-AC02-05CH11231. We gratefully acknowledge x-ray diffraction measurements by Wolter Siemons and Arturas Vailionis.

[1] M. Dawber, K. M. Rabe, and J. F. Scott, Rev. Mod. Phys. **77**, 1083 (2005).
[2] O. Auciello, J. Scott, and R. Ramesh, Phys. Today **51**, 22 (1998).
[3] D. D. Fong and C. Thompson, Annu. Rev. Mater. Res. **36**, 431 (2006).
[4] K. J. Choi *et al.*, Science **306**, 1005 (2004).
[5] A. M. Kolpak, I. Grinberg, and A. M. Rappe, Phys. Rev. Lett. **98**, 166101 (2007).
[6] Y. Yun and E. I. Altman, J. Am. Chem. Soc. **129**, 684 (2007).
[7] D. Li, M. H. Zhao, J. Garra, A. M. Kolpak, A. M. Rappe, D. A. Bonnell, and J. M. Vohs, Nature Mater. **7**, 473 (2008).
[8] R. Wang *et al.*, Phys. Rev. Lett. **102**, 047601 (2009).
[9] P. Maksymovych, S. Jesse, P. Yu, R. Ramesh, A. P. Baddorf, S. V. Kalinin, and I. J. Busch-Vishniac, Science **324**, 1421 (2009).
[10] A. T. Young, E. Arenholz, S. Marks, R. Schlueter, C. Steier, H. Padmore, A. Hitchcock, and D. G. Castner, J. Synchrotron Radiat. **9**, 270 (2002).
[11] C. Quitmann, U. Flechsig, L. Patthey, T. Schmidt, G. Ingold, M. Howells, M. Janousch, and R. Abela, Surf. Sci. **480**, 173 (2001).
[12] G. van der Laan and I. W. Kirkman, J. Phys.: Condens. Matter **4**, 4189 (1992).
[13] G. van der Laan, Phys. Rev. B **41**, 12366 (1990).
[14] G. van der Laan and B. T. Thole, Phys. Rev. B **43**, 13401 (1991).
[15] Hartree-Fock Slater integrals were scaled to 70% and intensities convoluted with Lorentzians of half width $\Gamma=0.08$, 0.48, and 0.8 eV in the $2p_{3/2}3d(t_2)$, $2p_{3/2}3d(e)+2p_{1/2}3d(t_2)$, and $2p_{1/2}3d(e)$ regions, respectively, to account for intrinsic lifetime broadening and with a Gaussian of $\sigma=0.14$ eV for instrumental broadening.
[16] K. Okada and A. Kotani, J. Electron Spectrosc. Relat. Phenom. **62**, 131 (1993).